Pergamon

Int. J. Heat Mass Transfer. Vol. 41, No. 11, pp. 1405–1415, 1998

Printed in Great Britain
0017-9310/98 $19.00+0.00

PII: S0017-9310(97)00268-8

The diffusion and P_1 approximations for modeling buoyant flow of an optically thick fluid

JEFFREY J. DERBY,† SIMON BRANDON‡ and ANDREW G. SALINGER§

Department of Chemical Engineering and Materials Science and Army HPC Research Center, University of Minnesota, Minneapolis, MN 55455-0132, U.S.A.

(*Received* 12 *September* 1996 *and in final form* 4 *September* 1997)

Abstract—Buoyant flow of an optically thick fluid representative of molten glass or an oxide crystal melt is solved via a finite element method using four different radiation models—the Rosseland diffusion approximation with and without radiation slip, the P_1 approximation, and a rigorous numerical treatment. The results indicate that both diffusion approximations fail to accurately predict thermal and flow fields in this problem due to their inability to represent thermal boundary layers. However, the P_1 approximation matches well with the rigorous numerical solution. This accuracy, coupled with implementation ease, favors the P_1 approximation for solution of problems of this type. © 1998 Elsevier Science Ltd. All rights reserved.

1. INTRODUCTION

Understanding heat transfer in fluids which absorb and emit radiant energy is a task complicated by the coupled, nonlinear physical phenomena of internal radiation [1] and natural convection [2]. There are several specific problems of scientific and technological interest in which heat transfer via radiation and convection occurs in optically thick liquids, such as the flow of the earth's mantle [3], the flow of oxide melts during crystal growth [4], and the processing of molten glass [5–12]. In the mathematical modeling of these problems, various approximations which rely on the short-range nature of radiant interactions have been commonly applied [13, 14]. The purpose of this study is to examine the performance of these approximations for modeling a representative problem of heat transfer and buoyant flow in optically thick fluids.

The general interaction of radiant heat transfer and natural convection in finite enclosures has received considerable attention. Larson and Viskanta [15] studied the effects of radiating walls in a two-dimensional rectangular enclosure filled with a totally transparent fluid. Lauriat [16] analyzed radiation heat transfer on the boundary layer regime in vertical slots of various aspect ratios. Webb and Viskanta [17] studied natural convection of a participating fluid in a rectangular cavity heated by incident radiant energy through a transparent side wall. Fusegi and Farouk [18] studied convection in a square enclosure for a wide range of Grashof and Prandtl numbers. Yücel *et al.* [19] and Tan and Howell [20] solved for flow of an absorbing, emitting, and scattering fluid in a differentially heated square enclosure. Salinger *et al.* [21] studied the effects of optical thickness and thermal gradients on the stability and structure of flows in a cylindrical container heated from below.

Molten glass processing is the most studied system involving the effects of internal radiation and fluid flow for optically thick fluids. Kellet [5, 6] was the first to show convincingly the importance of internal radiation through molten glass. Gardon [7] presented a comprehensive review of radiant heat transfer in glass. Noble *et al.* [8] modeled heat transfer and convection through a rectangular, two-dimensional enclosure representing an industrial glass melting furnace by employing the Rosseland diffusion approximation. Ungan and Viskanta [9] modeled three-dimensional convection in a glass melting tank using a diffusion approximation. Carvalho *et al.* [10] modeled heat transfer in molten glass using the diffusion approximation with a semi-empirical representation of boundary conditions. Murnane *et al.* [11] employed the commercial finite element code FIDAP to model the flow of molten glass in a melter using an effective thermal conductivity to account for radiant energy transfer. Roychowdhury and Srinivasan [12] modeled flows in the forehearth units of a glass tank furnace using a combination of optically thick and thin approximations.

In this study, we present a critical analysis of several common approximations for modeling conduction, convection, and radiation occurring in optically thick fluids. We analyze a problem representative of the buoyant flow of a molten glass or an oxide crystal growth melt in a cylindrical container heated from the side, which is described in Section 2. The flow problem is solved using standard finite element methodology, while the contributions from radiant energy transfer

† Author to whom correspondence should be addressed.
‡ Present address: Department of Chemical Engineering, Technion-Israel Institute of Technology, Haifa 32000, Israel.
§ Present address: Sandia National Laboratory, MS 1111, Alburquerque, NM 87185, U.S.A.

NOMENCLATURE

a	optical absorption coefficient
A	aspect ratio of cylinder
C_p	heat capacity
$\mathbf{e}_x$	unit vector in direction x
g	gravitational constant
Gr	Grashof number (defined in text)
i'	total directional radiant intensity
$\mathbf{I}$	identity tensor
J	irradiance
k	thermal conductivity
k_R	Rosseland radiant conductivity (defined in text)
l	radiant path length to boundary of participating medium
L	cylinder height
M	total number of mathematical degrees of freedom
n	refractive index
$\mathbf{n}$	unit vector pointing out of the participating medium
N	conduction-to-radiation parameter (defined in text)
N_T	total number of nodes in finite element mesh
N_p	total number of pressure unknowns
p	band-width of Jacobian matrix
P	dynamic pressure
Pr	Prandtl number (defined in text)
$\mathbf{q}_R$	radiant heat flux
r	radial coordinate
R	cylinder radius
T	temperature
$\mathbf{T}$	total stress tensor
$\mathbf{v}$	velocity vector
v_x	velocity component in direction x
z	axial coordinate.

Greek symbols

β	thermal expansivity
ΔT	temperature difference (defined in text)
ε	emissivity of walls
Θ	absolute temperature ratio (defined in text)
μ	viscosity
ρ	density
σ	Stefan–Boltzmann constant
τ	dimensionless absorption coefficient (optical thickness; defined in text)
Φ^i	biquadratic basis function
ψ	Stokes streamfunction
Ψ^i	discontinuous linear basis function
ω	solid angle.

Subscripts

0	reference value
h	hot
max	maximum value
r, z	components in coordinate directions
w	evaluated at wall.

Superscripts

i	finite element basis function index
(i)	finite element interpolant index
T	transpose
~	dimensional quantity.

Mathematical symbols

∇	divergence operator (defined in text)
$\cdot$	dot product.

are represented using several approaches—the Rosseland diffusion approximation with two different techniques for implementing boundary conditions, the P_1 approximation, as well as a rigorous finite element solution of the radiant transfer equation. These solution methodologies are outlined in Section 3. The results, shown in Section 4 and discussed in Section 5, clearly show the shortcomings of the Rosseland diffusion approximations for modeling heat transfer coupled with buoyant flow in an optically thick fluid. The P_1 approximation predicts the temperature and flow field much more accurately for the sample problem considered here.

2. PROBLEM DEFINITION

We consider axisymmetric, steady flows driven by buoyancy within a cylinder with rigid, black walls. The cylinder is completely filled by an incompressible, Newtonian fluid with constant thermophysical properties. This fluid is considered to be semi-transparent with gray radiant properties. The scattering of radiation by the fluid is assumed to be unimportant and is not considered.

The steady-state, incompressible Navier–Stokes equations, with the body force term represented by the Boussinesq approximation, are coupled with the energy balance equation, given in dimensionless forms by

$$(\mathbf{v}\cdot\nabla)\mathbf{v} = \nabla\cdot\mathbf{T} + \frac{Gr}{\Theta}(T-1)\mathbf{e}_z \tag{1}$$

$$\nabla\cdot\mathbf{v} = 0 \tag{2}$$

$$(\mathbf{v}\cdot\nabla)T = \frac{1}{Pr}\left(\nabla^2 T - \frac{\tau}{4N}\nabla\cdot\mathbf{q}_R\right) \tag{3}$$

where $\mathbf{v}$ is the fluid velocity, $\nabla \equiv \mathbf{e}_r \partial/\partial r + \mathbf{e}_z \partial/\partial z$ is the gradient operator with $(\mathbf{e}_r, \mathbf{e}_z)$ denoting unit vectors in the cylindrical coordinate system, $\mathbf{T}$ is the total stress tensor, T is dimensionless temperature, and $\mathbf{q}_R$ represents the flux of radiant energy through the fluid. The dimensionless groups Gr, Pr, τ, N, and Θ are discussed below. The total stress tensor $\mathbf{T}$ appears above in equation (1) and is defined for a Newtonian fluid as

$$\mathbf{T} = -P\mathbf{I} + (\nabla \mathbf{v} + (\nabla \mathbf{v})^T) \tag{4}$$

where P is the dynamic pressure, $\mathbf{I}$ is the identity tensor, $\nabla \mathbf{v}$ is the dyadic product of the gradient operator and the velocity vector, and the superscript T denotes the transpose operation.

In the above equations, the velocity and dynamic pressure fields are scaled with $\mu/\rho L$ and $\mu^2/\rho L^2$, respectively, where μ is the viscosity of the fluid, ρ is the fluid density, and L is the height of the cylinder. The radial and axial coordinates are made dimensionless by scaling with L. The temperature field is nondimensionalized by $T \equiv \bar{T}/T_0$, where $\bar{T}$ is the absolute temperature and T_0 is the reference temperature, which is taken to be the minimum temperature applied to the cylinder surface. The radiant flux vector $\mathbf{q}_R$ is scaled by $n^2\sigma T_0^4$, where n is the index of refraction of the fluid and σ is the Stefan–Boltzmann constant.

The Grashof number, Gr, is a measure of the buoyant force acting upon the fluid and is defined as

$$Gr = \frac{\rho^2 g L^3 \beta \Delta T}{\mu^2} \tag{5}$$

where g is the gravitational constant and β is the thermal expansivity of the fluid. The temperature difference across the cylinder is defined as $\Delta T \equiv T_h - T_0$, with T_h denoting the maximum temperature applied to the cylinder surface. The Prandtl number, defined as

$$Pr = \frac{\mu C_p}{k} \tag{6}$$

is the ratio of viscous to thermal diffusivity; C_p is the fluid heat capacity, and k is the thermal conductivity. The remaining parameters arise from the radiation terms. The optical thickness,

$$\tau = aL \tag{7}$$

with a representing the optical absorption coefficient of the gray fluid, is a measure of the transparency of the medium to infrared radiation and is assumed independent of wavelength. The conduction-to-radiation parameter is defined as

$$N = \frac{ka}{4n^2\sigma T_0^3}. \tag{8}$$

The dimensionless conduction-to-radiation parameter naturally appears in the radiant terms and is a rough measure of the relative importance of conduction heat transfer with respect to radiant transport in an optically thick medium. Finally, the ratio of the temperature difference applied across the system to the reference temperature is defined to be

$$\Theta = \frac{\Delta T}{T_0}. \tag{9}$$

The aspect ratio of the container is considered to be unity, so the axial and radial coordinates range between zero and one. No-slip and no-penetration conditions are specified for the velocity field along all walls of the cylinder, and axisymmetry is imposed along the centerline,

$$v_r = v_z = 0, \quad 0 \leqslant r \leqslant 1, \quad z = 0, 1 \tag{10}$$

$$v_r = v_z = 0, \quad r = 1, \quad 0 \leqslant z \leqslant 1 \tag{11}$$

$$v_r = \partial v_z/\partial r = 0, \quad r = 0, \quad 0 \leqslant z \leqslant 1. \tag{12}$$

We consider that the container top and bottom are cool and isothermal and that the side-wall is heated with a parabolic temperature distribution. This particular choice of boundary conditions represents a general condition of side-heating in a cylindrical geometry and was motivated after the work of Baumgartl *et al.* [22]. These thermal conditions are given in dimensionless form as

$$T = 1, \quad 0 \leqslant r \leqslant 1, \quad z = 0 \tag{13}$$

$$T = 1, \quad 0 \leqslant r \leqslant 1, \quad z = 1 \tag{14}$$

$$T = 1 + 4z(1-z)\Theta, \quad r = 1, \quad 0 \leqslant z \leqslant 1. \tag{15}$$

The total normal heat flux is prescribed to be zero along center axis by symmetry,

$$\mathbf{e}_r \cdot \left(\nabla T - \frac{\tau}{4N} \mathbf{q}_R \right) = 0, \quad r = 0, \quad \leqslant z \leqslant 1. \tag{16}$$

3. SOLUTION METHODOLOGY

3.1. *Radiant transport*

The divergence of the radiant flux vector represents the contribution of internal radiant transfer to the energy balance of equation (3) and is given by [14]

$$\nabla \cdot \mathbf{q}_R = \tau \left[4T^4 - \int_{\omega=0}^{4\pi} i'(\omega)\, d\omega \right] \tag{17}$$

where i' is the dimensionless radiant intensity (scaled by $n^2\sigma T_0^4$) and ω is the solid angle of a spherical geometry centered at the point of interest.

The dependence of the radiant intensity on the solid angle, ω, is given by

$$i'(\omega) = i'_w(\omega) \exp[-\tau l(\omega)] + \frac{\tau}{\pi} \int_0^l T^4(l^*) \exp[-\tau(l-l^*)]\, dl^* \tag{18}$$

where l denotes the distance from the domain boundaries to the point of interest along the solid angle ω

and l^* is a dummy variable of integration. The first term on the right-hand side of equation (18) represents the intensity coming from the boundaries, while the integral term accounts for the contributions from the intervening fluid.

The intensity emanating from the boundaries in the case of black (non-reflecting) walls is simply

$$i'_w(\omega) = \frac{T_w^4}{\pi}. \tag{19}$$

The more general expression for $i'_w(\omega)$ in the case of gray walls has been considered in past analyses using the rigorous radiation method discussed in the next section; see, e.g., [23–26]. While the assumption of black walls simplifies the current analysis, this choice is also appropriate for the test problem considered here. Black walls magnify the importance of radiant fluxes near the wall and therefore represent a challenging test case for the problem at hand. Highly reflecting walls represent another challenge for solution accuracy of the global radiation field; however, this case is not considered here.

Accounting for radiation energy transfer introduces significant complications into the equation of change of energy. The inclusion of equations (17)–(19) converts equation (3) to an integro-differential equation which is extremely challenging to solve. Viskanta and Anderson [1] and Siegel and Howell [14] present many approaches for solving this equation; advances in methodologies are also discussed by Chan [27] and Howell [28]. For our test problem involving an optically thick medium, we employ four different methods to account for radiant heat transfer. These approaches are described below.

3.1.1. *Rosseland diffusion approaches.* These approaches rely on the short-range nature of radiant interactions in an optically thick medium, so that the radiant flux vector can be approximated as [13, 14]

$$\tilde{\mathbf{q}}_R = -\frac{16n^2\sigma\tilde{T}^3}{3a}\nabla\tilde{T} = -k_R\nabla\tilde{T} \tag{20}$$

where k_R is the radiant conductivity defined as

$$k_R = \frac{16n^2\sigma\tilde{T}^3}{3a} \tag{21}$$

and the tilde represents a dimensional quantity.

Now the former integro-differential energy equation, equation (3), is simplified to a nonlinear partial differential equation by using the above radiant conductivity to combine the conductive and radiant fluxes to yield the following dimensionless equation,

$$(\mathbf{v}\cdot\nabla)T = \frac{1}{Pr}\nabla\cdot\left(1+\frac{4T^3}{3N}\right)\nabla T. \tag{22}$$

The model problem posed above is solved using the field equations (1) and (2) coupled with this new energy equation (22).

While the Rosseland diffusion approximation yields a single, consistent set of field equations, there are at least two different manners in which to apply boundary conditions. The first approach, which refer to subsequently as the no-slip method, is to directly apply the conditions specified in equations (13)–(15) for the wall temperatures.

The second approach attempts to remedy the fact that the diffusion approximation breaks down near system boundaries. In this approach, which we refer to as the slip method, we specify an effective boundary temperature to allow for a discontinuity, or slip [14], of the temperature field as the boundary is approached. We employ the particular approximation introduced by Howell and Goldstein [29], which was derived using asymptotic expansions to match linearized solutions near the wall with the diffusion solution far from the wall in a conduction–radiation problem. Using this approach, we replace the boundary temperatures of equations (13)–(15) with extrapolated temperatures obtained from a slip coefficient which depends only on the conduction-to-radiation parameter. For the sake of brevity, we omit the details of this standard approach; the interested reader is referred to [14] and [29] for further information.

3.1.2. P_1 *approach.* The P_1 approximation (also known as the differential and Milne–Eddington approximations [14]) relies on reducing the integral terms of the radiation transfer equation to differential terms via a finite set of moment equations. Using this approximation, we replace the integral of the radiant intensity in equation (17) with the irradiance $J(r, z)$ [1] to give the following nondimensional expression,

$$\nabla\cdot\mathbf{q}_R = \tau[4T^4 - J(r,z)]. \tag{23}$$

As in the previous analyses, the former integro-differential energy equation (3) is again simplified to a nonlinear partial differential equation to yield

$$(\mathbf{v}\cdot\nabla)T = \frac{1}{Pr}\left(\nabla^2 T - \frac{\tau^2}{4N}[4T^4 - J(r,z)]\right). \tag{24}$$

The partial differential moment equation for the irradiance is given by

$$\nabla^2 J = 3\tau^2[J(r,z) - 4T^4]. \tag{25}$$

The model problem is now solved using the original field equations (1) and (2) coupled with the new energy equation (24) and the irradiance equation (25). While the P_1 formulation introduces one more field variable $J(r, z)$ and an additional partial differential equation (25) to the analysis, the extra computational effort involved for solution is modest, particularly compared to the costs of solving an integro-differential equation (see Section 3.2).

Unlike the Rosseland diffusion approximation discussed above, there is no ambiguity about boundary conditions for the P_1 approximation. Boundary conditions for the temperature field are applied directly from the prescribed wall temperature distributions,

equations (13)–(15). The boundary conditions for the additional irradiance equation (25) are prescribed along all the black walls as

$$-\mathbf{n}\cdot\nabla J=\frac{3\tau}{2}[J_w(r,z)-4T_w^4], \tag{26}$$

where $\mathbf{n}$ is the outward-pointing normal along each surface and the subscript w denotes the value of the indicated variable at the wall. A symmetry condition is supplied along the system centerline,

$$\mathbf{e}_r\cdot\nabla J=0. \tag{27}$$

3.1.3. *Rigorous approach.* In this approach, we apply the finite element method of Brandon and Derby [23, 24] to evaluate the radiant contributions of the above equations explicitly. While the details of this formulation are omitted here (interested readers are referred to the references above), the major features include the evaluation of the integral expressions of equations (17) and (18) using localized spherical coordinate systems, repeated Gaussian quadrature, and self-consistent interpolation of the temperature field via a finite element basis. This scheme represents a numerical solution of the exact integro-differential equation set (1)–(3) and is capable of representing radiant heat transfer of any optical thickness. In addition, the scheme is highly accurate, flexible, and robust [23, 24].

The disadvantage of this approach is that it is quite computationally intensive. Therefore, of particular importance for this problem is the utilization of a cost-effective approximation technique, based on the method of Swartz and Wendroff [30] to reduce the overall computational burden associated with calculating the radiant terms. Since the system geometry is fixed, the geometrical portion of the radiation integrals can be computed once and stored; see [21, 24, 31] for more details. This procedure is similar in spirit to the zonal method of Hottel [32], but it can be applied in a self-consistent manner to the higher-order approximations of the temperature field employed by finite element methods.

3.2. *Discretization via the finite element method*

We apply the Galerkin finite element method [33, 34] to solve for the dimensionless velocity, pressure, and temperature fields. The axisymmetric computational domain is discretized using two-dimensional, quadrilateral elements, and the velocity field, temperature field, and irradiance field (for the P_1 approximation) are expanded by nine-node, Langrangian biquadratic basis functions, $\Phi^i(r,z)$, in the following manner,

$$\mathbf{v}(r,z)=\sum_{i=1}^{N_T}\begin{bmatrix}v_r^{(i)}\mathbf{e}_r\\ v_z^{(i)}\mathbf{e}_z\end{bmatrix}\Phi^i(r,z) \tag{28}$$

$$T(r,z)=\sum_{i=1}^{N_T}T^{(i)}\Phi^i(r,z) \tag{29}$$

$$J(r,z)=\sum_{i=1}^{N_T}J^{(i)}\Phi^i(r,z)$$

(for the P_1 approximation only) (30)

where N_T is the number of nodes in the mesh and $v_r^{(i)}$, $v_z^{(i)}$, $T^{(i)}$, and $J^{(i)}$ represent the interpolated velocity component, temperature, and irradiance values at each node. The dynamic pressure in the fluid is approximated by discontinuous linear basis functions [35, 36],

$$P(r,z)=\sum_{i=1}^{N_p}P^{(i)}\Psi^i(r,z) \tag{31}$$

where N_p is the number of pressure unknowns (three per element). This mixed-order formulation (sometimes called the Q2P1 or 9/3 element [35]) has been demonstrated to be particularly efficient when used with the Galerkin finite element method to solve for incompressible flows [36–40].

The Galerkin method is used to form a set of weighted residuals which discretize the original integro-differential equations (for the rigorous method) or partial differential equations (for the diffusion and P_1 methods), and boundary conditions are applied in the standard manner [33, 34]. The weighted residuals are integrated numerically using Gauss–Legendre quadrature to form a large set of nonlinear algebraic equations, which are solved using a full Newton–Raphson iterative technique employing a direct matrix solver [41]. All elements of the Jacobian matrix are calculated analytically.

A regular 8×8 mesh of 64 biquadratic elements and 1059 mathematical unknowns (1348 mathematical unknowns for the P_1 approximation) is employed for all calculations shown here. This discretization was judged to be numerically convergent based on prior analyses of buoyant flows of radiantly participating fluids [39]. For this discretization, approximately 7 CPU s (12 CPU s for the P_1 method) on the Cray X-MP of the Minnesota Supercomputer Center are needed per Newton iteration to solve the field equations, with 4–6 Newton iterations to obtain a fully converged solution (for all methods).

The computational effort expended for each Newton iteration is dominated by the direct LU decomposition of the Jacobian matrix arising from this strongly coupled, non-linear problem. The LU decomposition scales with the total problem size (M) and the bandwidth (p) of the Jacobian matrix as $\mathcal{O}(Mp^2)$ [41]. Since these did not change for the two implementations of the Rosseland diffusion methods, the effort needed for these methods was identical. As indicated above, additional effort was needed for the P_1 approach due to the extra degrees of freedom associated with discretization of the irradiance. For the rigorous approach, the Jacobian matrix is in theory quite dense, and its decomposition would require $\mathcal{O}(M^3)$ operations for the general case. However, for an optically

Table 1. Dimensionless parameters and groups

Description	Symbol and definition	Value
Aspect ratio	$A = L/R$	1
Emissivity of walls	ε_w	1
Absolute temperature ratio	$\Theta = (T_h - T_0)/T_0$	1/3
Prandtl number	$Pr = \mu C_p/k$	500
Conduction-to-radiation number	$N = ka/(4n^2\sigma T_0^3)$	0.1
Optical thickness	$\tau = aL$	10
Grashof number	$Gr = \rho^2 g L^3 \beta \Delta T/\mu^2$	0–2060

thick medium, as is considered here, the rapid decay of the exponentials in the radiation intensity integral, equation (18), enables the use of certain 'cut-off' criteria to decide when it is appropriate to ignore the contribution of certain terms (see [24] for a detailed explanation of this procedure). The use of these cut-off criteria and the inherently large bandwidth already imposed by discretization of the velocity and pressure fields resulted in a negligible increase in the bandwidth of the Jacobian matrix, thus yielding nearly identical CPU times for the solution of the rigorous method compared with the Rosseland diffusion approaches. However, there was an additional one-time calculation requiring approximately 60 CPU s to evaluate the Swartz–Wendroff radiation factors for the rigorous approach (see the prior discussion in Section 3.1.3).

4. RESULTS AND DISCUSSION

We perform calculations using the four radiant heat transfer models on the problem described above and with a set of thermophysical properties which are representative of molten glass or an oxide crystal growth melt. These properties are listed in Table 1. To consider the effect of differing driving forces for buoyant flow, we vary the dimensionless Grashof number as the primary variable in this study.

A comparison of these methods for the case of no flow, $Gr = 0$, is shown in Fig. 1, where isotherms indicate the temperature field throughout the cylindrical domain. Heat flows from the outer cylindrical wall ($r = 1$ on the right-hand-side of the domains) toward the upper and lower surfaces ($z = 0$ and $z = 1$). There is no flux of heat across the cylinder centerline ($r = 0$ on the left-hand-side of the domains) due to the symmetry condition imposed there. Without convection there is also symmetry of the temperature field about the $z = 0.5$ plane. The temperature field predicted with the P_1 method is very similar to that predicted by the rigorous treatment, while there are noticeable differences in the Rosseland diffusion methods.

These differences are made clearer in Fig. 2, where the axial temperature profiles for each case are shown at the radial position midway between centerline and wall. Notice again that the temperature profile is symmetric about $z = 0.5$. In this plot, the difference between the P_1 model prediction and the profile computed with the rigorous treatment are virtually indistinguishable. Both solutions capture the boundary layer region near the wall where both conduction and radiation are important. In contrast, neither of the solutions obtained with the Rosseland methods compare well over the entire domain. The Rosseland model with slip matches the profile predicted by the rigorous treatment reasonably well, except near the walls at $z = 0$ and $z = 1$. The no-slip Rosseland model matches only at the walls.

Figures 3 and 4 show temperature and flow fields, respectively, predicted by each model for the case of conduction, radiation, and significant levels of convection, $Gr = 2060$. The distorted temperature fields displayed in Fig. 3 are very different than those of the no flow cases and are caused by the effects of counterclockwise convective flow cell. The temperature field through the middle portion of the domain is vertically stratified, with nearly horizontal isotherms, and thermal boundary layers have formed along the outer cylinder walls and the centerline. As in the prior $Gr = 0$ cases, the temperature fields predicted by the rigorous treatment and the P_1 model show very good agreement. The predictions by the Rosseland diffusion models are qualitatively similar to the rigorous solution but quantitatively different, especially that of the no-slip approach.

Also evident in the thermal fields predicted by the rigorous and P_1 models are small oscillations in the solution near the vertical wall and centerline boundary layers. These oscillations or 'wiggles' are commonly observed in solutions to transport problems obtained using the Galerkin finite element method and broadcast a signal regarding the accuracy of the solutions [42]. Since the objective of this study was to directly compare the performance of the various formulations under comparable discretizations, we did not pursue an extensive study of this issue. We comment further on the significance of resolving thermal boundary layers in problems such as those posed here in the ensuing section.

The flows in this system are driven by horizontal thermal gradients; the primary counterclockwise flow is up along the heated outer wall and down at the centerline, as shown by streamlines of the dimen-

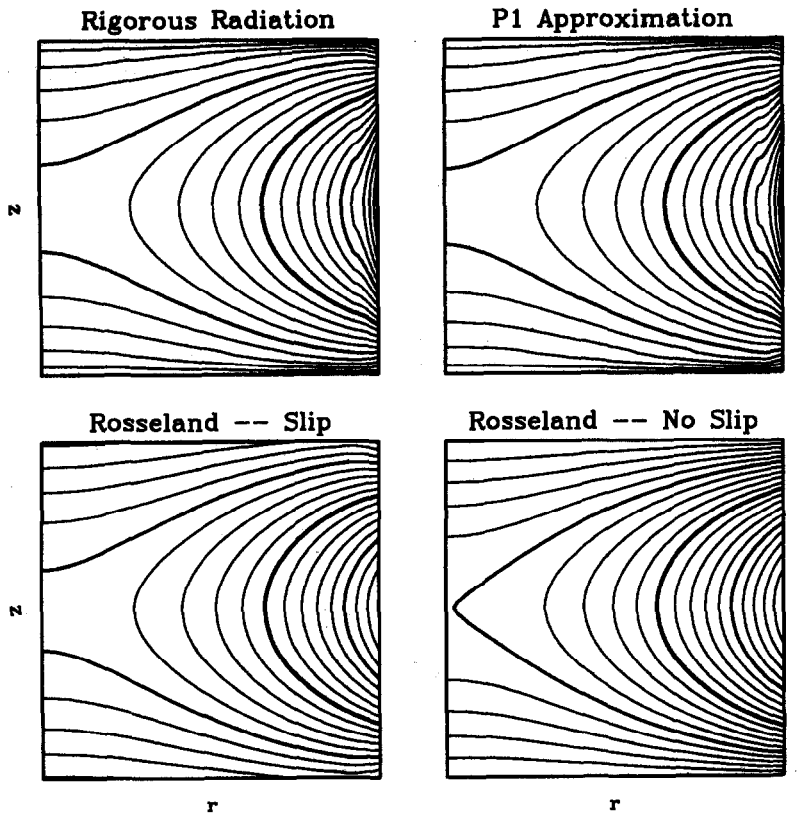

Fig. 1. The temperature fields predicted by each model are shown for the case of no flow, $Gr = 0$, by 20 isotherms plotted evenly between T_h (at $r = 1$, $z = 0.5$) and T_0 (along top and bottom surfaces). Every fifth isotherm is represented by a bold line.

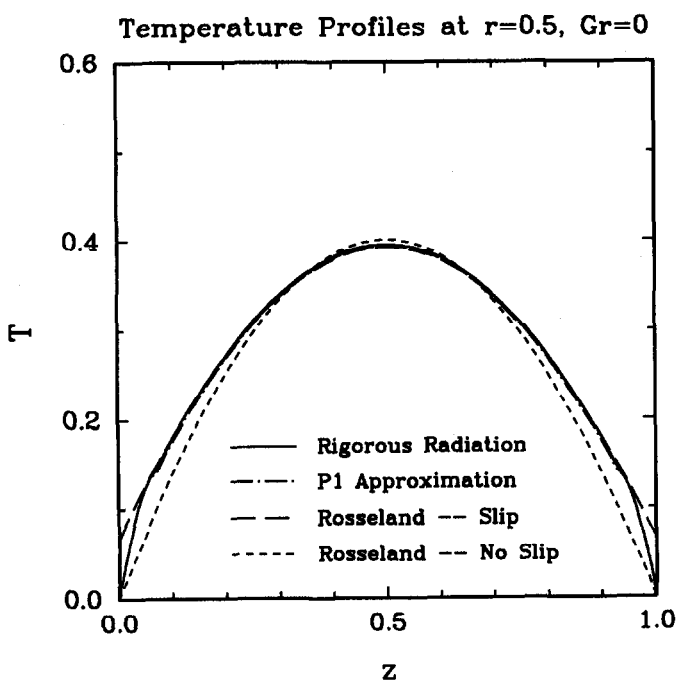

Fig. 2. The axial temperature profile midway between the centerline and side wall ($r = 0.5$) is shown for each model for the case of no flow, $Gr = 0$. The zero plotting temperature corresponds to T_0, while T_h corresponds to unity.

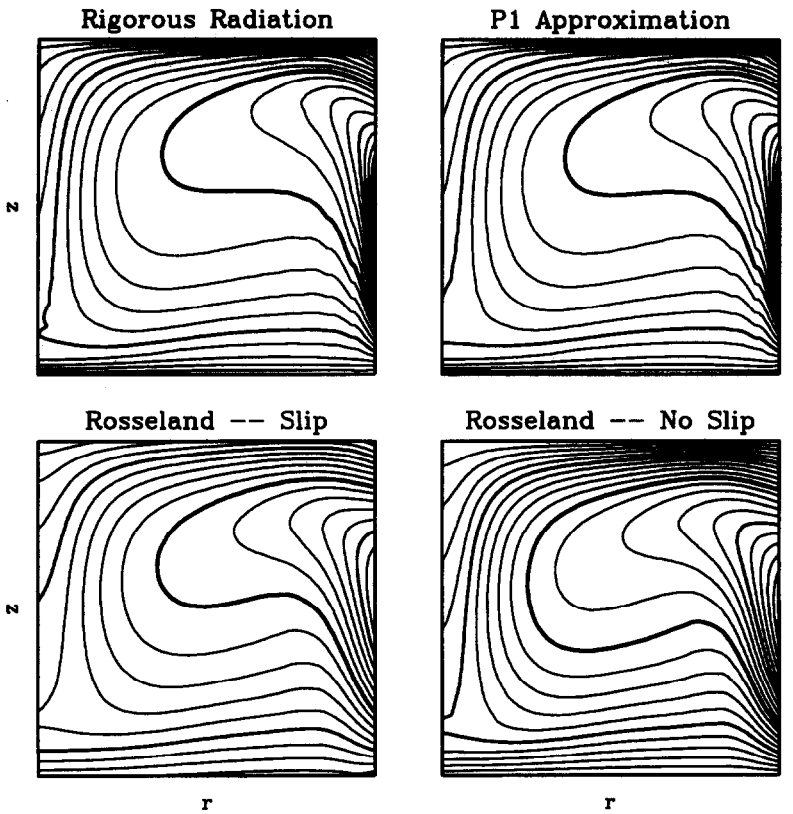

Fig. 3. The temperature fields predicted by each model are shown for the case strong flow, $Gr = 2060$, by 20 isotherms plotted evenly between T_h (at $r = 1$, $z = 0.5$) and T_0 (along top and bottom surfaces). Every fifth isotherm is represented by a bold line.

sionless Stokes streamfunction $\psi(r, z)$ in Fig. 4. In addition, a very weak Moffat eddy [43], which flows in a clockwise direction, is nested in the upper corner of the ampoule. The structure of the flows predicted by all models is very similar, yet the strength of the flows varies considerably. The maximum streamfunction is indicative of the strength of these flows and ranges from $\psi_{max} = 0.21$ for the rigorous treatment to $\psi_{max} = 0.29$ for the no-slip Rosseland model.

The axial temperature profiles predicted for each model are shown at the radial position midway between centerline and wall for the $Gr = 2060$ case in Fig. 5. Under the influence of the strong flow inward across the top surface and outward along the bottom, the temperature profiles are skewed toward $z = 1$. For this case, the P_1 approximation continues to match well the rigorous solution. Although there are some deviations between the two predictions within the bulk of the domain, the P_1 method solution closely tracks the rigorous temperature profile near the top and bottom surfaces. The solutions obtained with the Rosseland methods do not compare well with that from the rigorous treatment. While the Rosseland model with slip tracks near the rigorous solution in the bulk, it does not resolve the thermal boundary layers near the surfaces. The no-slip Rosseland model matches only at the walls and significantly over-predicts temperatures through the bulk.

5. CONCLUSIONS

We have implemented four different approaches to solve for radiation energy transport within an optically thick fluid which is experiencing buoyancy-driven flow. This problem was constructed to feature coupled heat transfer via conduction, internal radiation, and natural convection in a system qualitatively similar to those encountered in molten glass processing or the growth of an oxide crystal from the melt. The choice of any one of the solution methods will depend upon implementation ease, computational effort needed for solution, and the accuracy of the solution. Only a limited number of cases are considered in this study, nevertheless the results clearly suggest some recommendations.

The Rosseland approximations were easy to implement and economical in computing needs. These issues are especially important with regard to incorporating internal radiant heat transfer into existing heat transfer codes (see, e.g., [11]). However, this simplicity carries with it a significant source of inaccuracy—the inability of this method to capture the

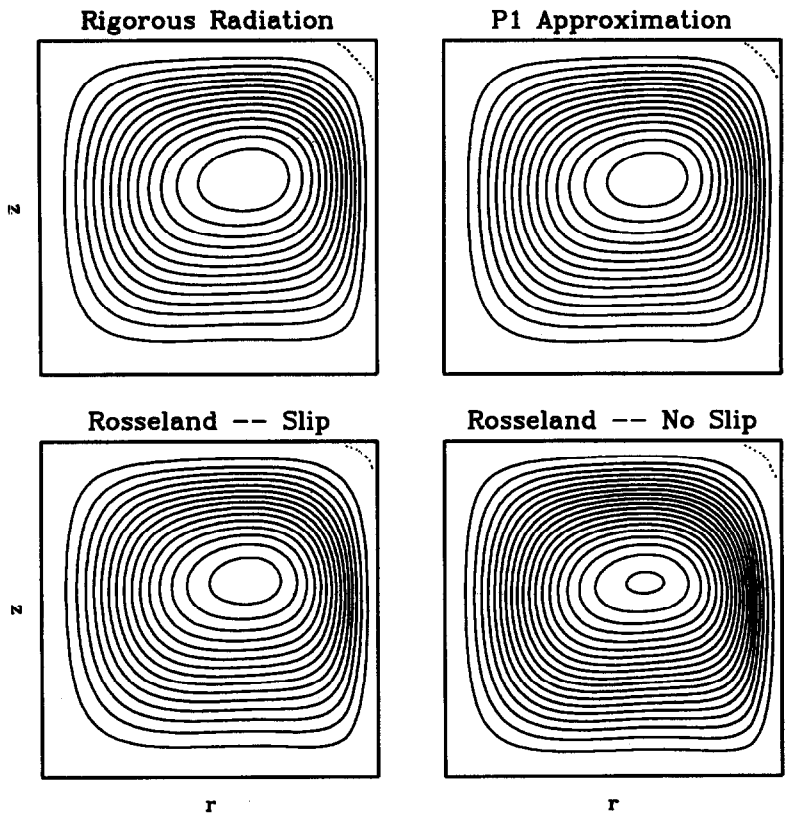

Fig. 4. The flow fields predicted by each model are shown for the case of strong flow, $Gr = 2060$. Streamlines are drawn with a uniform spacing of $\Delta\psi = 0.015$ with the zero streamline indicated by a dotted line. Streamfunction maxima are $\psi_{max} = 0.21$ for the rigorous solution, $\psi_{max} = 0.22$ for the P_1 method solution, $\psi_{max} = 0.23$ for the Rosseland model with radiation slip, and $\psi_{max} = 0.29$ for the Rosseland model with no radiation slip.

physics of the thermal boundary layer near walls. Indeed, this downfall may lead to significant error, especially in systems such as this where the thermal boundary layers are important for driving flow. Of the two implementations, the Rosseland method with slip is the more accurate in matching temperature profiles away from the system boundaries. However, this is not an endorsement for the Rosseland slip approach, since the accuracy of this method will likely continue to degrade with increased convection and progressively sharper boundary layers.

The P_1 method is slightly more difficult to implement than the Rosseland diffusion methods, since it requires solving an additional coupled partial differential equation for an additional field variable, the irradiance. Also, the computational effort needed to solve with the P_1 method is slighter greater than that needed for the Rosseland diffusion methods. However, this effort is significantly less than solution of the original integro-differential energy equation via the rigorous treatment, since the new set of equations are coupled partial differential equations, whose solution is readily computed. For the problem considered here, the P_1 approximation yielded surprisingly accurate results compared to the solutions obtained from the rigorous treatment. Of course, it is well known that the P_1 approximation is valid for optically thick media; e.g., Ratzel and Howell [44] showed that the P_1 approximation performed poorly for media not optically thick in a study of radiant and conduction energy transfer in a gray absorbing and emitting medium. This restriction may become increasingly important for modeling systems which exhibit intense flows. Vigorous convection will lead to large gradients in the thermal field as the temperature of well-mixed bulk connects with the wall temperature through thin boundary layers. When the width of these boundary layers approaches the length scale of the mean free path for radiation, namely $1/a$, one would expect that the optically thick approximation, upon which the P_1 approximation relies [14, 44], would break down and lead to significant error.

The rigorous calculation using the method of Brandon and Derby [23, 24] requires significant effort for implementation as well as computation of solutions. However, the payoff is a method which computes accurate results for media of any optical thickness. This feature may also be important for accurately computing heat transfer at convection levels still higher than those considered here where very thin

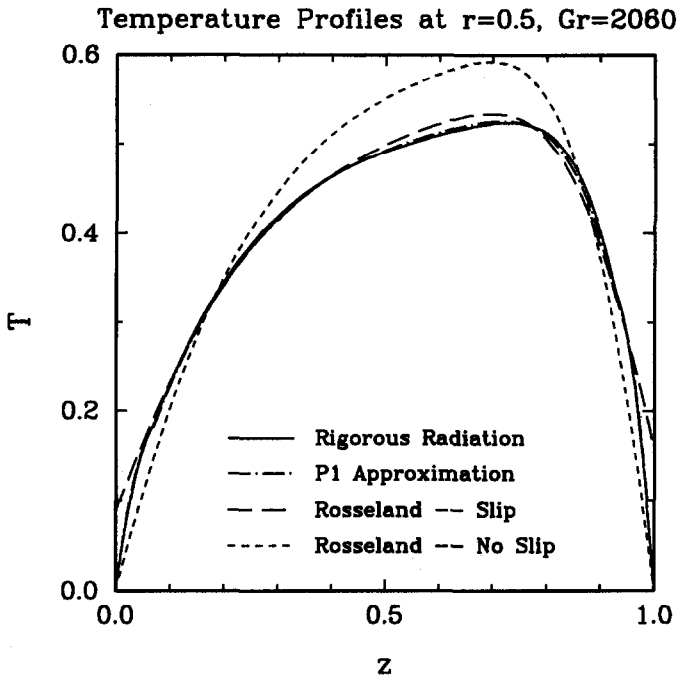

Fig. 5. The axial temperature profile midway between the centerline and side wall ($r = 0.5$) is shown for each model for the case of strong flow, $Gr = 2060$. The zero plotting temperature corresponds to T_0, while T_h corresponds to unity.

boundary layers occur, as discussed in the preceding paragraph.

Based on the results of this analysis, we advocate the use of the P_1 formulation for the solution of buoyant flows in optically thick fluids, such as those encountered in glass processing or oxide melt crystal growth systems, with the proviso that extremely intense convective flows may require special considerations. While not as easily implemented as the Rosseland diffusion formulations nor as accurate for the general radiation problem as rigorous numerical methods, this approach proved optimal for the problem studied here in terms of algorithmic implementation, computational costs, and solution accuracy.

Acknowledgements—This work was supported in part by the National Science Foundation under grant number DMR-9058386 and the Microgravity Sciences Program of the National Aeronautics and Space Administration. Computational resources were provided by the University of Minnesota Supercomputer Institute and the Army High Performance Computing Research Center under the auspices of the Department of the Army, Army Research Laboratory cooperative agreement DAAH04-95-2-0003/contract DAAH04-95-C-0008, the content of which does not necessarily reflect the position or policy of the government, and no official endorsement should be inferred. We also wish to thank K. Edwards for timely help in assembling the figures for this manuscript.

REFERENCES

1. Viskanta, R. and Anderson, E. E., Heat transfer in semi-transparent solids. In *Advances in Heat Transfer*, Vol. 11, ed. T. F. Irvine and J. P. Hartnett. Academic Press, New York, 1975.
2. Bejan, A., *Convection Heat Transfer*. Wiley-Interscience, New York, 1984.
3. Matyska, C., Moser, J. and Yuen, D. A., The potential influence of radiative heat transfer on the formation of megaplumes in the lower mantle. *Earth Planet. Sci. Lett.*, 1994, **125**, 255–266.
4. Rosenberger, F. E., *Fundamentals of Crystal Growth I: Macroscopic Equilibrium and Transport Concepts*. Springer-Verlag, Berlin, 1979.
5. Kellet, B. S., Transmission of radiation through glass in tank furnaces. *J. Soc. Glass Technol.*, 1952, **36**, 115–123.
6. Kellet, B. S., The steady flow of heat through hot glass. *J. Opt. Soc. Amer.*, 1952, **42**, 339–343.
7. Gardon, R., A review of radiant heat transfer in glass. *J. Amer. Ceram. Soc.*, 1961, **44**, 305–312.
8. Noble, J. J., Clomberg, L. A., Sarofim, A. F. and Hottel, H. C., Mathematical experimental modeling of the circulation patterns in glass melts. *Journal of Heat Transfer*, 1972, **94**(5), 149–154.
9. Ungan, A. and Viskanta, R., Three-dimensional numerical modelling of circulation and heat transfer in a glass melting tank. *Glastech. Ber.*, 1987, **60**, 71–78 and 115–124.
10. Carvalho, M. G., Oliveira, P. and Semiao, V. A., Three-dimensional modelling of an industrial furnace. *Journal of the Institute of Energy*, Sept. 1988.
11. Murnane, R. A., Johnson, W. W. and Moreland, N. J., The analysis of glass melting processes using three-dimensional finite elements. *International Journal for Numerical Methods in Fluids*, 1988, **8**, 1491–1511.
12. Roychowdhury, A. P. and Srinivasan, J., The modelling of radiation heat transfer in forehearth units in glass melting. *Warme- und Stoffübertragung—Thermo and Fluid Dynamics*, 1994, **30**(2), 71–75.
13. Rosseland, S., *Theoretical Astrophysics; Atomic Theory*

and the Analysis of Stellar Atmospheres and Envelopes. Clarendon Press, Oxford, 1936.
14. Siegel, R. and Howell, J. R., *Thermal Radiation Heat Transfer*, 2nd edn. McGraw-Hill, New York, 1981.
15. Larson, D. W. and Viskanta, R., Transient combined laminar free convection and radiation in a rectangular enclosure. *Journal of Fluid Mechanics*, 1976, **78,** 65–85.
16. Lauriat, G., Combined radiation-convection in gray fluids enclosed in vertical cavities. *Journal of Heat Transfer*, 1982, **104,** 609–615.
17. Webb, B. W. and Viskanta, R., Analysis of radiation-induced natural convection in rectangular enclosures. *Journal of Thermophysics*, 1987, **1,** 146–153.
18. Fusegi, T. and Farouk, B., Laminar and turbulent natural convection-radiation interactions in a square enclosure filled with a nongray gas. *Numerical Heat Transfer, Part A*, 1989, **15,** 303–322.
19. Yücel, A., Acharya, S. and Williams, M. L., Natural convection and radiation in square enclosures. *Numerical Heat Transfer Part A*, 1989, **15,** 261–278.
20. Tan, Z. and Howell, J. R., Combined radiation and natural convection in a two-dimensional participating square medium. *International Journal of Heat and Mass Transfer*, 1991, **34,** 785–793.
21. Salinger, A. G., Brandon, S., Aris, R. and Derby, J. J., Buoyancy-driven flows of a radiatively participating fluid in a vertical cylinder heated from below. *Proc. R. Soc. Lond. A*, 1993, **442,** 313–341.
22. Baumgartl, J., Budweiser, W., Müller, G. and Neumann, G., Studies of buoyancy driven convection in a vertical cylinder with parabolic temperature profile. *Journal of Crystal Growth*, 1989, **89,** 9–17.
23. Brandon, S. and Derby, J. J., A finite element method for internal radiative heat transfer and its application to analysis of the growth of semitransparent crystals. In *Fundamentals of Radiation Heat Transfer*, HTD-Vol. 160, ed. W. A. Fiveland, A. L. Crosbie, A. M. Smith and T. F. Smith. ASME, New York, 1991, pp. 1–16.
24. Brandon, S. and Derby, J. J., A finite element method for conduction, internal radiation, and solidification in a finite axisymmetric enclosure. *International Journal of Numerical Methods for Heat and Fluid Flow*, 1992, **2,** 299–333.
25. Brandon, S. and Derby, J. J., Internal radiative transport in the vertical Bridgman growth of semitransparent crystals. *Journal of Crystal Growth*, 1991, **110,** 481–500.
26. Brandon, S. and Derby, J. J., Heat transfer in vertical Bridgman growth of oxides: effects of conduction, convection, and internal radiation. *Journal of Crystal Growth*, 1992, **121,** 473–494.
27. Chan, S. H., Numerical methods for multidimensional radiative transfer analysis in participating media. *Annual Review of Numerical Fluid Mechanics and Heat Transfer*, 1987, **1,** 305–350.
28. Howell, J. R., Thermal radiation in participating media: the past, the present, and some possible futures. *Journal of Heat Transfer*, 1988, **110,** 1220–1229.
29. Howell, J. R. and Goldstein, M. E., Effective slip coefficients for coupled conduction-radiation problems. *Journal of Heat Transfer*, 1969, **91**(1), 165–166.
30. Swartz, B. and Wendroff, B., Generalized finite-difference schemes. *Math. Comp.*, 1969, **23,** 37–49.
31. Kuppurao, S. and Derby, J. J., Finite element formulations for accurate calculation of radiant heat transfer in diffuse-gray enclosures. *Numerical Heat Transfer, Part B: Fundamentals*, 1993, **24,** 431–454.
32. Hottel, H. C. and Cohen, E. S., Radiant heat exchange in a gas-filled enclosure: Allowance for nonuniformity of gas temperature. *AIChE J.*, 1958, **4,** 3–14.
33. Strang, G. and Fix, G. J., *An Analysis of the Finite Element Method.* Prentice-Hall, Inc., Englewood Cliffs, NJ, 1973.
34. Hughes, T. J. R., *The Finite Element Method.* Prentice-Hall, Inc., Englewood Cliffs, NJ, 1987.
35. Gresho, P. M., Contribution to Von Karman Institute lecture series on computational fluid dynamics: advection–diffusion and Navier–Stokes equations. *UCRL-92275*, Lawrence Livermore National Laboratory, Livermore, CA, 1985.
36. Engleman, M. S., Sani, R. L., Gresho, P. M. and Bercovier, M., Consistent vs. reduced integration penalty methods for incompressible media using several old and new elements. *International Journal for Numerical Methods in Fluids*, 1982, **2,** 25–42.
37. Winters, K. H., Laminar natural convection in a partially divided rectangular cavity at high Rayleigh number. *International Journal for Numerical Methods in Fluids*, 1988, **8,** 247–281.
38. Sackinger, P. A., Brown, R. A. and Derby, J. J., A finite element method for analysis of fluid flow, heat transfer and free interfaces in Czochralski crystal growth. *International Journal for Numerical Methods in Fluids*, 1989, **9**(4), 453–492.
39. Salinger, A. G., Aris, R. and Derby, J. J., Finite element formulations for large-scale, coupled flows in adjacent porous and open fluid domains. *International Journal for Numerical Methods in Fluids*, 1994, **18,** 1185–1209.
40. Derby, J. J., Brandon, S., Salinger, A. G. and Xiao, Q., Large-scale numerical analysis of materials processing systems: high-temperature crystal growth and molten glass flows. *Comput. Methods Appl. Mech. Engng*, 1994, **112,** 69–89.
41. Dalquist, G. and Björck, Å., *Numerical Methods*, translated by Anderson, N. Prentice-Hall, Inc., Englewood Cliffs, NJ, 1974.
42. Gresho, P. M. and Lee, R. L., Don't suppress the wiggles—they're telling you something. *Computers and Fluids*, 1981, **9,** 223–253.
43. Moffat, H. K., Viscous and resistive eddies near a sharp corner. *Journal of Fluid Mechanics*, 1964, **18,** 1–18.
44. Ratzel III, A. C. and Howell, J. R., Two-dimensional radiation in absorbing–emitting media using the P–N approximation. *ASME Journal of Heat Transfer*, 1983, **105,** 333–340.